2018 IEEE International Conference on Robotics and Automation (ICRA)
May 21-25, 2018, Brisbane, Australia

LineDrone Technology: Landing an unmanned aerial vehicle on a power line

François Mirallès,* Philippe Hamelin, Ghislain Lambert, Samuel Lavoie,
Nicolas Pouliot, Matthieu Montfrond and Serge Montambault

Hydro-Québec, Varennes, QC, Canada

***Abstract*—This paper presents the design of a multirotor unmanned aerial vehicle (UAV) capable of landing semi-automatically on a power line while carrying a payload. The vehicle then rolls along the line to perform an inspection. Special attention is given to the vehicle's onboard vision system, which consists of a monocular camera and LiDAR used together to compute the pose of the vehicle relative to the power line. Landing assistance is provided to the pilot by a position-based visual controller that aligns and keeps the vehicle centered along the power line. The pilot remains in control of vertical and longitudinal movement during descent. The proposed approach was tested on a full-scale test line and shows promise for future applications of high value to the electric industry such as non-destructive testing of power transmission lines.**

I. Introduction

Early approaches to power line inspection by unmanned aerial vehicles (UAVs) date back to the late 1980s [1] but only in the last decade did intensive research on UAV technology finally yield workable commercial solutions for electric power utilities. It is now possible to take very high-quality images of power transmission lines and their components at a much lower cost. UAVs still have untapped potential in performing tasks very close to, or even in contact with, line components [2][3], e.g., non-destructive testing or repair applications of power transmission lines [4].

Such tasks, typically performed by teams of qualified line technicians, have also been carried out in the past decade by line-suspended robots [5]. Of course, robots must then be mounted on the power line following standard line maintenance procedures. If a UAV could carry a significant payload directly onto energized lines and land there in a reliable, safe and robust manner, it is thus anticipated that several high-value inspection and maintenance tasks could be performed more efficiently. Achieving this is the main objective set and currently pursued under "LineDrone", a comprehensive UAV project initiated at IREQ.

This paper presents the project's first major technical milestone, i.e., the design and control of a multirotor UAV capable of bringing a payload of up to 5 kg onto a power line. Once landed on the conductor, the UAV simply rolls along the power line to perform an inspection. The first target application is to measure the level of galvanic protection remaining on the steel strands of the power line. This correlates closely to the remaining life of the conductors and is thus potent data for optimizing power utility asset management. An earlier paper [6] explains the problem of galvanic loss and presents the IREQ-developed LineCore sensor, which is light enough to be carried by LineDrone.

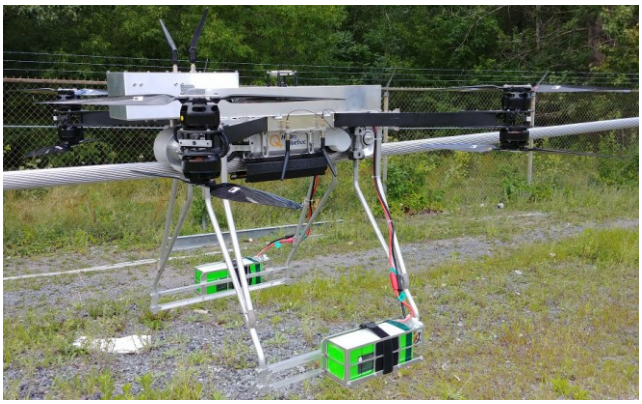

Figure 1. Vehicle landed on a power line.

For the target mission, the UAV must be flown very close to a power transmission line. Though a skilled pilot could in theory do this, operating conditions may often make this impracticable. At the usual working distance of 30 m and more, it is difficult to judge the position of the UAV relative to the power line and ensure safe, robust operation. Wind gusts pose an additional challenge to the pilot. Furthermore, the best locations for piloting the UAV may be inaccessible. In practice, the pilot thus needs some level of assistance to reliably perform the task.

To assist the pilot, a vision system made of a camera and LiDAR estimates the pose of the UAV relative to the power line. This estimate is used in a position-based visual control loop that aligns the UAV along the power line. The pilot remains in control of the UAV's altitude and the longitudinal position, as well as procedure initialization and emergency termination.

The contributions of this paper are threefold:

- Introduction of a new UAV that lands on a power line and then rolls along it to perform an inspection.
- Description of a vision system and two algorithms to compute UAV pose relative to the power line.

*Corresponding author: miralles.francois@ireq.ca.

François Mirallès, Philippe Hamelin, Ghislain Lambert, Samuel Lavoie, Nicolas Pouliot, Matthieu Montfrond and Serge Montambault are with the Robotics, Inspection and Maintenance department of Hydro-Québec's research institute (IREQ), Varennes, Québec, J3X 1S1, Canada, e-mail: {miralles.francois, hamelin.philippe, lambert.ghislain, lavoie.samuel, pouliot.nicolas , montfrond.matthieu, montambault.serge}@ireq.ca.

- Results from full-scale outdoor tests showing that the proposed UAV with its vision system is able to land on a power line safely under moderate wind conditions.

II. Related work

To place a payload on a power line, two robotic tasks can be distinguished: perching and landing. To the authors' knowledge, the first attempt to perch a UAV on a power line was carried by [7] in collaboration with the Air Force Research Laboratory. The system uses an original mode of sensing: the magnetic field emitted by an energized power line is used as an input to the UAV navigation system. However, such a system can only perch on live lines. To cover the requirements of all applications of UAVs to power line maintenance, a UAV must be able to place a payload on either a live or "dead" line.

Later research teams working on perching on, and more generally on maneuvering around, cylindrical structures turned to sensing solutions based on a camera and IMU in a visual servoing control loop. Successful perching by sensing cylindrical objects, potentially a power line, has been reported [8]. Interesting results have been achieved for the inspection of pole-like structures, a very high frame rate being attained thanks to a computationally efficient line tracking algorithm [9]. Vehicle position was initially controlled with a position-based visual controller but the authors later performed the same application with an image-based visual controller [10]. In this project, a position-based visual controller is used for simplicity.

External illumination conditions make sensing more difficult when part of the object appears very bright while the shaded part is very dark [11]. This is particularly true for cylindrical objects such as power line conductors. The edge of the object to be tracked may also be less apparent depending on the background. Since such constraints are faced in this project, and as a safety measure, LiDAR technology complements the camera in viewing the power line.

In the literature that deals directly with power line detection [12-15], the UAV is usually at a distance such that the power line is about 2 pixels wide. On top of computing time, the usual challenges for the detection algorithms are background noise removal, connectivity when a power line is detected as multiple segments and multiple lines being detected when one power line is present. In our case, as the camera gets closer and closer during the decent, the power line first is 1 pixel wide but increases to up to 50 pixels. Early on in the project, it was found acceptable to detect only a segment of the power line in order to compute the relative pose of the camera. As a first step in the development of a solution, GPU technology was then used to run a well-established but computationally intensive algorithm for ridge detection [16]. Finally, the extended Kalman filter and measurement gating techniques give greater reliability than an approach purely based on image analysis.

A UAV landing on a distribution line ground wire and then rolling along it to perform a visual inspection is described in a patent [17] and video [18]. This system so far seems to be the closest in design to LineDrone but its level of autonomy during landing remains unclear. Due to greater distances, heights and wind gusts, the application requires a much higher level of assistance to the pilot. Simply put, the operating conditions and the intensive magnetic field around very-high-voltage transmission lines can make a safe landing difficult or infeasible in a purely manual mode. Although the UAV should be able to land on a live line, no such landing is covered in this paper. Experiments on electromagnetic interference shielding have already been run by the authors [19] and landing on a live line is a goal that the final system will soon achieve under this research project.

III. System overview

A commercial UAV base frame was modified to meet the requirements of the task. Fig. 1 is a picture of the vehicle when landed on a mockup power line. Fig. 2 is a diagram of the architecture of the system. The UAV weighs 14 kg without the payload and measures $1.12 \times 1.12 \times 0.63$ m in width, depth and height. One vehicle capability required is to place an active payload on a power line. An active payload is any instrument that can collect measurements related to the power line.

The task is to place a payload on an ACSR (aluminum conductor steel reinforced) power line conductor with a voltage rating of 315 to 735 kV. Such conductors vary in diameter from 19 to 35 mm. It was thus not necessary to design a gripper suited to diameters outside that range. Instead, a multifunctional landing gear was designed. It comprises two legs and a set of wheels. The legs carry the batteries and are funnel-shaped to help align the vehicle in the final phase of landing.

The Pixhawk autopilot [20] is used as a low-level flight controller (LLFC) and keeps the vehicle stable in flight. In the flight mode used for the experiments, its navigation system relies only on an IMU and a barometer. A compass is not used since it would be unreliable near a live line.

An Nvidia Tegra TX1 embedded computer acts as a high-level flight controller (HLFC) and performs functions directly related to the landing task:

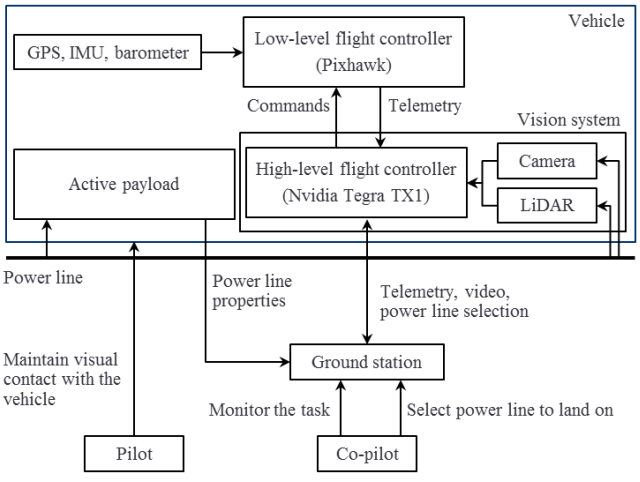

Figure 2. System architecture.

- process measurements from the vision system to compute the pose of the camera relative to the power line,
- compute the required roll angle and yaw rate to align the vehicle along the power line and transmit the command to the LLFC,
- transmit the telemetry and video signals to the ground station.

The vision system consists of a monocular camera and LiDAR rigidly fixed together at the front of the vehicle. No gimbal is used in order to keep the system simpler and lighter. Both the camera and LiDAR point downward.

Knowing actual ACSR diameters, it would have been possible with just a camera to estimate the distance to the power line by measuring its width in the image. Depending on the time of day and weather, however, the ACSR may not be illuminated uniformly, one side appearing brighter than the other. It was thus decided to use a LiDAR to enhance robustness under varying illumination and for redundancy. The LiDAR projects a rotating laser point in a plane that intersects the power line and measures at least one 3D point on it. The camera measures the projection of the power line in the image. An extended Kalman filter (EKF) computes the pose of the camera relative to the power line by combining LiDAR and camera measurements.

Decoupled linear controllers operating in Cartesian space compute the roll and yaw rate commands to align the vehicle along the power line. By having the pilot align the vehicle approximately along the power line before activating the algorithm, it can be assumed that the yaw error converges quickly to a small value. Hence, a roll command should be sufficient for the controller to control the lateral position and the pilot remains in control of the longitudinal position using the pitch command, in addition to the vehicle's altitude.

Since there may be several power lines in the image, to initiate landing on the right one, the co-pilot first clicks near it on the ground station display. This triggers the image processing that detects and tracks the power line, and computes the pose of the vehicle. The pilot brings the vehicle down towards the power line while the co-pilot monitors the landing by checking the telemetry and video signals. When the vehicle is in contact with the power line, the pilot turns off the engines. If necessary, the pilot can move the UAV forward or backward on the power line using its motorized wheels, a much less energy-intensive phase of the mission. Lastly, the ground station software controls the collection of inspection results from the active payload.

In the next section, the two procedures to compute the pose of the camera are discussed: the first is an algebraic method, and the second uses an EKF.

IV. Vision System Design

A. Image processing

The goal of image processing, after manual selection of the relevant power line, is to locate and track that line in the image during the landing task while the distance between the vehicle and power line is from 6 to 10 m. To give a better idea of the problem at hand, Fig. 3 shows two images of a

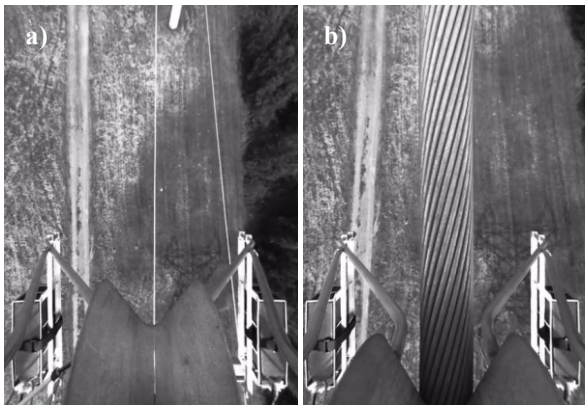

Figure 3. Images of the power line at 10 m (a) and after landing (b)

power line taken by the onboard camera, one when 10 m away and the other once landed. At 10 m, the power line appears in the image as a ridge 1 pixel wide. As the vehicle descends, the ridge widens to reach a width of up to 50 pixels after landing.

Ridge detection is a well-studied problem in the computer vision literature. The method presented in [16] is used to detect the centerline and width of the ridge. Parts of the ridge detection algorithm are computationally heavy, namely, image convolution with the Gaussian kernels and ridge map computation. These computations are executed on the GPU of the Tegra TX1 while the other steps run on the CPU.

The power line is detected as the longest ridge and must be sufficiently straight. Other criteria could be chosen for more robustness. The ridge points selected are used to compute a line $\mathbf{L}$ defined by points $\mathbf{A}$ and $\mathbf{B}$, as seen in Fig. 4b.

The LiDAR point on the power line is taken as the closest in distance.

B. Algebraic pose computation

Pilot assistance is provided by the HLFC, which aligns the $\mathbf{X}$-axis of the vehicle frame along the power line. The vision system is insensitive to movements along the power line (longitudinally) and the actual roll angle ϕ and pitch angle θ are provided by the navigation system of the LLFC.

Using the symbols defined in Table I and reference frames in Fig. 4, the problem is to estimate the partial state vector of the camera relative to the power line:

$$\mathbf{X}=[\psi \quad y \quad z]^T \tag{1}$$

The line at the center of the ridge is defined by:

$$[\mathbf{L}]_I=[\mathbf{A}]_I\times[\mathbf{B}]_I \tag{2}$$

where $\mathbf{A}$ and $\mathbf{B}$ are two image points on the detected power line in homogeneous coordinates.

A line in the image backprojects to a plane in 3D space [21]:

$$[\boldsymbol{\pi}]_C=\mathbf{K}^T[\mathbf{L}]_I \tag{3}$$

where $\mathbf{K}$ is the projection matrix of the camera in homogeneous coordinates:

$$\mathbf{K}=\begin{bmatrix}\alpha_u & 0 & u_0 & 0\\ 0 & \alpha_v & v_0 & 0\\ 0 & 0 & 1 & 0\end{bmatrix} \quad (4)$$

and $\boldsymbol{\pi}$ a plane represented as $\boldsymbol{\pi}=[\mathbf{n} \quad d]^T$. d is the distance from $\boldsymbol{\pi}$ to the frame's origin. The normal vector $\mathbf{n}$ to plane $\boldsymbol{\pi}$ can be expressed in the leveled vehicle frame:

$$[\mathbf{n}]_{VL}=\mathrm{Rot}_V^{VL}.\mathrm{Rot}_C^V.[\mathbf{n}]_C=[a \quad b \quad c]^T \quad (5)$$

with $\mathrm{Rot}_V^{VL}=\mathrm{Rot}(\mathbf{Y},\theta).\mathrm{Rot}(\mathbf{X},\phi)$ and Rot_C^V is a known calibrated value. The leveled vehicle frame has the same origin and yaw angle as the vehicle frame, but a roll and pitch equal to zero.

The yaw angle of the camera relative to the power line is computed by projecting the normal $[\mathbf{n}]_{VL}$ onto $\mathbf{X_P}$:

$$\psi=\mathrm{acos}(a) \quad (6)$$

The full rotation matrix representing the orientation of the camera relative to the power line is:

$$\mathrm{Rot}_V^P=\mathrm{Rot}(\mathbf{Z},\psi).\mathrm{Rot}(\mathbf{Y},\theta).\mathrm{Rot}(\mathbf{X},\phi) \quad (7)$$

$\mathrm{Rot}(\mathbf{X},\phi)$, $\mathrm{Rot}(\mathbf{Y},\theta)$ and $\mathrm{Rot}(\mathbf{Z},\psi)$ are the rotation around **X-**, **Y-** and **Z-**axes respectively.

$\left[\mathbf{t}_V^P\right]_P$ is computed using LiDAR point $\mathbf{D}$ on the power line, in homogeneous coordinates with:

$$[\mathbf{D}]_V=\mathbf{T}_C^V.\mathbf{T}_L^C.[\mathbf{D}]_L \quad (8)$$

$$\left[\mathbf{t}_V^P\right]_P=-\mathrm{Rot}_V^P.[\mathbf{D}]_V \quad (9)$$

where $\mathbf{T}_C^V$ and $\mathbf{T}_L^C$ are calibrated values.

Alternatively, a 3D point on the power line can be measured from the camera image, based on the known diameter of the power line and measured line width in image. An assumption worth mentioning is that the slope (grade) of the power line is small (< 15°), the method assuming that the power line conductor is horizontal.

C. Pose computation by filtering

The pose of the camera can be estimated with an extended Kalman filter as explained below. The pose can be described by the process

$$\mathbf{X}_k=\mathbf{A}\mathbf{X}_{k-1}+\mathbf{W}_{k-1} \quad (10)$$

where $\mathbf{X}=\left[\psi \ \dot{\psi} \ y \ \dot{y} \ z \ \dot{z}\right]^T$ represents camera position and velocity, $\mathbf{W}_{k-1}$ is the process noise, and 6×6 matrix $\mathbf{A}$ relates the state vector at the previous time step $k-1$ to the state vector at time step k. A simple constant-velocity model was chosen for $\mathbf{A}$ [22]:

$$\mathbf{A}=\begin{bmatrix}\Lambda & 0 & 0\\ 0 & \Lambda & 0\\ 0 & 0 & \Lambda\end{bmatrix} \quad \Lambda=\begin{bmatrix}1 & T\\ 0 & 1\end{bmatrix} \quad (11)$$

where T represents the filter sampling time.

Measurement vector $\mathbf{Z}$ is governed by the equation

$$\mathbf{Z}_k=\mathbf{H}(\mathbf{X}_k,\mathbf{V}_k) \quad (12)$$

where $\mathbf{V}_k$ is the measurement noise, and $\mathbf{H}$ is a nonlinear measuring function derived hereafter.

TABLE I. NOMENCLATURE FOR THE SYMBOLS USED IN THE TEXT.

Symbols	Description
{I}, {P}, {L}, {C}, {V}, {VL}	Frames respectively attached to the image, power line, LiDAR, camera, vehicle and leveled vehicle
$\mathbf{X}$	A point, a vector, or a matrix
$[\mathbf{X}]_A$	A point or a vector expressed in frame A
$(\mathbf{O}_A, \mathbf{X}_A, \mathbf{Y}_A, \mathbf{Z}_A)$	Three-dimensional frame A
$(\mathbf{O}_I, \mathbf{u}, \mathbf{v})$	Image frame
Rot_B^A	Rotation matrix corresponding to the orientation of frame B relative to frame A
$\left[\mathbf{t}_B^A\right]_C=[x \ y \ z]^T$	Translation vector of frame B relative to A expressed in frame C
$\mathbf{T}_B^A$	Rigid transformation from frame B to frame A
α_u, α_v	Focal length of the camera, in pixels
u_0, v_0	Principal point of the camera, in pixels
ϕ, θ, ψ	Roll, pitch and yaw angles of the camera

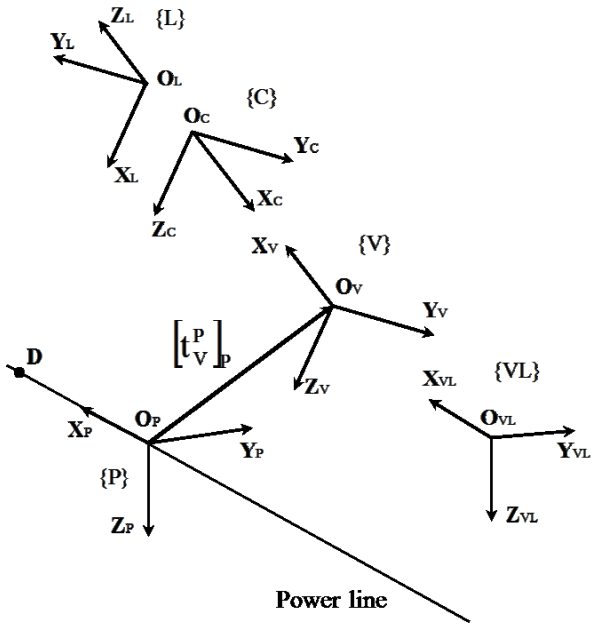

(a)

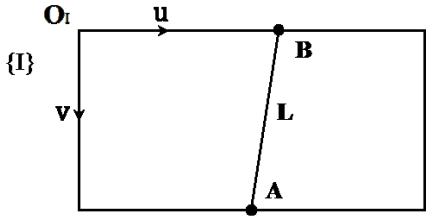

(b)

Figure 4. Frames involved in the pose computation (a) and synthetic image (b).

The process and measurement noise are assumed to be independent and to follow a Gaussian distribution:

$$p(\mathbf{W}) \approx N(0,\mathbf{Q}) \tag{13}$$

$$p(\mathbf{V}) \approx N(0,\mathbf{R}) \tag{14}$$

where $\mathbf{Q}$ and $\mathbf{R}$ are the process and measurement noise covariance matrices, respectively. N represents a Gaussian distribution. Following [22], $\mathbf{Q}$ is

$$\mathbf{Q}=\begin{bmatrix}\mathbf{\Gamma} & \mathbf{0} & \mathbf{0}\\ \mathbf{0} & \mathbf{\Gamma} & \mathbf{0}\\ \mathbf{0} & \mathbf{0} & \mathbf{\Gamma}\end{bmatrix} \quad \mathbf{\Gamma}=\begin{bmatrix}\frac{1}{3}T^3 & \frac{1}{2}T^2\\ \frac{1}{2}T^2 & T\end{bmatrix} \tag{15}$$

Taking $\mathbf{e}_k=\hat{\mathbf{X}}_k-\mathbf{X}_k$ as the estimate error, the EKF minimizes the expected value of the squared error $E[\mathbf{e}_k\mathbf{e}_k^T]$.

$\mathbf{Z}$ is a column vector that comprises the LiDAR point on the power line, noted $[\mathbf{D}]_L$ and the projection of the power line in the image, noted $[\mathbf{L}]_I$. When possible, the width $[w]_I$ of the power line in the image can be included in $\mathbf{Z}$:

$$\mathbf{Z}=[[\mathbf{D}]_L \quad [\mathbf{L}]_I \quad [w]_I]^T \tag{16}$$

The LiDAR plane is contained in the $(\mathbf{O}_L,\mathbf{X}_L,\mathbf{Y}_L)$ plane and can be represented with just its normal vector $\mathbf{Z}_L$. The power line can be represented by a point $[\mathbf{O}_P]_P=[0 \quad 0 \quad 0]^T$ and a vector $[\mathbf{X}_P]_P=[1 \quad 0 \quad 0]^T$.

Using $\mathbf{T}_P^L=\mathbf{T}_C^L\mathbf{T}_V^C\mathbf{T}_P^V$ to transform the power line parameters in the LiDAR frame, $[\mathbf{D}]_L$ is computed with

$$s=\frac{-[\mathbf{Z}_L]_L.[\mathbf{O}_P]_L}{[\mathbf{Z}_L]_L.[\mathbf{X}_P]_L} \tag{17}$$

$$[\mathbf{D}]_L=[\mathbf{O}_P]_L+s[\mathbf{X}_P]_L \tag{18}$$

The projection of the power line in the image is computed with Plücker coordinates as a representation of lines in 3D space, similar to [9]:

$$\mathbf{L}=\mathbf{A}\mathbf{B}^T+\mathbf{B}\mathbf{A}^T \tag{19}$$

where $\mathbf{A}$ and $\mathbf{B}$ are two 3D points on the power line in homogeneous coordinates:

$$\begin{aligned}\mathbf{A}&=[0 \quad 0 \quad 0 \quad 1]^T\\ \mathbf{B}&=[1 \quad 0 \quad 0 \quad 1]^T\end{aligned} \tag{20}$$

The power line can be expressed in the camera frame with the estimated value of $\mathbf{T}_P^C$. Finally, a line in 3D space projects to a line in the image [21]:

$$[\mathbf{l}]_{\times I}=\mathbf{K}.[\mathbf{L}]_C.\mathbf{K}^T \tag{21}$$

with $[\mathbf{l}]_\times$ the matrix form of a 2D line $\mathbf{l}=[l_1 \quad l_2 \quad l_3]^T$:

$$[\mathbf{l}]_\times=\begin{bmatrix}0 & l_3 & l_2\\ l_3 & 0 & -l_1\\ -l_2 & l_1 & 0\end{bmatrix} \tag{22}$$

$\mathbf{l}$ is normalized so that $l_3=1$, making $[\mathbf{L}]_I$ a two-element vector:

$$[\mathbf{L}]_I=[l_1/l_3 \quad l_2/l_3]^T \tag{23}$$

The width of the power line in the image is computed with

$$[w]_I=(2\alpha_u r)/\hat{z} \tag{24}$$

with r the radius of the power line and $\hat{z}$ the estimated vertical position of the vehicle relative to the power line.

$[\mathbf{D}]_L$, $[\mathbf{L}]_I$ and $[w]_I$ are independent measurements so corresponding updates to the state estimate $\hat{\mathbf{X}}_k$ are applied sequentially. Erroneous measurements are gated using [22]

$$\mathbf{v}_k^T\mathbf{S}_k^{-1}\mathbf{v}_k \leq \gamma \tag{25}$$

with the innovation $\mathbf{v}_k=\mathbf{Z}-\hat{\mathbf{Z}}$, the innovation covariance $\mathbf{S}_k=\frac{\partial \mathbf{H}}{\partial \mathbf{X}_k}\mathbf{P}_{k+1|k}\frac{\partial \mathbf{H}^T}{\partial \mathbf{X}_k}+\mathbf{R}$, the gate threshold γ and $\mathbf{P}_{k+1|k}$ the a priori covariance. γ follows a chi-squared distribution and is computed given a certain number of degrees of freedom and probability of rejecting the true measurement. In this case, since $\mathbf{H}$ is non-linear, (25) is an approximation.

V. Control

The LLFC installed on the vehicle runs *ArduCopter* firmware [23]. Though the LLFC supports full-position-control flight modes, they are not usable near power lines because compass readings are strongly affected by electromagnetic interference. One functional flight mode, known as "Altitude Hold", ensures tracking of a target roll, pitch and yaw rate denoted ϕ_d, θ_d and $\dot{\psi}_d$ respectively. The altitude is also stabilized by the LLFC and the set point can be changed by the pilot through a desired climb rate $\dot{z}_d$. The *ArduCopter* firmware was modified to support commands from the HLFC through the Mavlink serial protocol [24].

As stated in Section II, the roll and yaw rate commands of the vehicle suffice for the controller to align the $\mathbf{X}$-axis of the camera with the power line, thus leaving the altitude and pitch commands to the pilot. The role of the HLFC is hence to provide a target roll angle ϕ_d and a target yaw angle rate $\dot{\psi}_d$, which become set points for the LLFC. Fig. 5 illustrates this proposed control architecture involving the pilot, LLFC and HFLC.

Assuming a small yaw angle ψ, the vehicle's lateral position and yaw angle can then be seen as two single-input-single-output (SISO) systems, the lateral position y and yaw angle ψ being mapped directly to the roll command ϕ_d and the yaw rate command $\dot{\psi}_d$ respectively. Moreover, thanks to the EKF defined in Cartesian space, from the controller perspective, the system dynamics is the same for the whole work envelop, which would not be the case if an image-based approach had been used. This led to choosing decoupled linear controllers for the lateral position and yaw angle, which are presented in Fig. 6.

The LLFC and vehicle's dynamics relating the target yaw rate $\dot{\psi}_d$ to the actual yaw angle ψ intrinsically include at least one integrator. For such a Type 1 system, there is no need to include an integrator in the controller to obtain a zero steady state error for a constant reference. Hence, a simple proportional controller was selected to control the yaw angle, with $k_{p\psi}$ being the proportional gain.

The dynamics relating target roll angle ϕ_d to lateral position y also reflects a Type 1 system. However, this cannot be relied upon to obtain a steady state error in the presence of

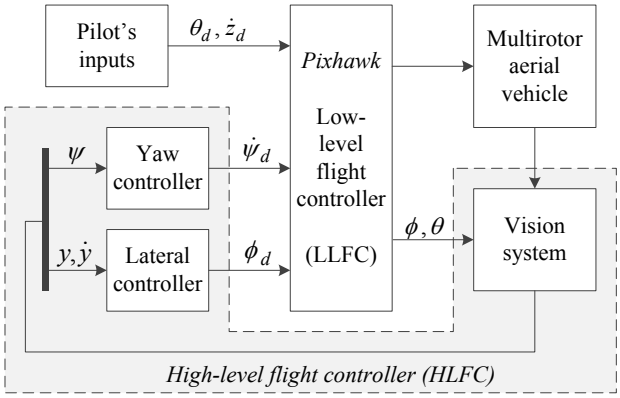

Figure 5. Controller architecture

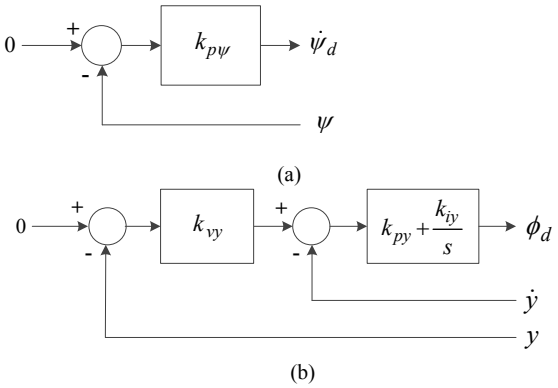

Figure 6. Block diagram of (a) the yaw controller and (b) the lateral controller.

disturbances such as lateral wind, which in practice affect the position more than the yaw angle. Since the EKF provides a smooth estimate of lateral position y and lateral velocity ẏ, a cascaded P/PI controller was considered. This controller has proven its robustness in many industrial applications, including in visual servoing of a UAV [25]. The inner loop velocity PI controller is parameterized with k_{py} and k_{iy}, which are respectively the proportional and integral gains. The outer loop position controller is strictly defined by the proportional gain k_{vy}.

VI. Test Results

First, the work envelop of the vehicle is characterized. Distances to the power line as measured by the camera and LiDAR are then compared. Results of landing on a test power line outside the laboratory are shown, first under ideal conditions and second under more challenging conditions (see accompanying video).

A. Work envelop

The work envelop is defined by the zone above the power line where the camera can view the line. The pilot must bring the UAV into this zone and the controller must keep it there until landed. The UAV is assumed to reach a maximum positive roll angle of 15° when to the left and -15° when to the right of the power line. The camera is a FLIR Chameleon3 with a 1/2-inch CMOS. The lens is a Sunex DSL388B with a 2.7-mm focal length. The LiDAR is a Hokuyo UTM-30LX with a fan angle of 270°. From Fig. 7, it can be seen that the large field of view of the vision system

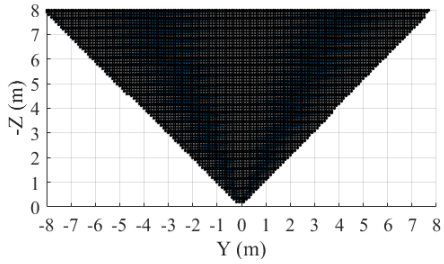

Figure 7. Work envelop of the UAV.

gives the pilot and controller a large margin to complete the task.

B. Influence of camera resolution on distance estimation

The camera resolution is 1280 × 1024 pixels and it is matched to a wide-angle lens. The power line thus appears very thin in the image at higher altitudes. Fig. 8 shows the theoretical perceived thickness of a power line 35 mm in diameter as a function of viewing distance. At a distance of about 8.8 m, the perspective projection model of the camera predicts that the power line will be 1 pixel wide. A variation of +0.1 pixel leads to a decrease of 0.8 m in the distance to the power line. Ridge width estimation must thus be very accurate and fairly precise to estimate the distance to the power line correctly.

Fig. 9 compares the estimated vertical distance to the power line based on ridge width measurement $[w]_I$ to the vertical distance computed with the EKF using only the LiDAR measurement $[\mathbf{D}]_L$ and cable projection in the image $[\mathbf{L}]_I$. Above 1.7 m, it is not possible to measure the vertical distance to the power line using the ridge width in the image. Below 1.7 m, the ridge width measurement becomes sufficiently accurate, the average difference with the EKF using the LiDAR being 0.05 m and the maximum error being 0.2 m.

C. Field results

Power line measurement in the image from the camera and by the LiDAR are both influenced by illumination conditions in different ways. Closer to the power line, it becomes more difficult to reliably measure its thickness from the image. Firstly, since part of the line may appear brighter and the shaded part darker, the ridge detector underestimates power line thickness. Secondly, the appearance of the power line deviates from a ridge as individual strands become visible.

LiDAR measurements are reliable at closer distances but strong sunlight can momentarily prevent any measurement at longer distances, thus limiting its usability.

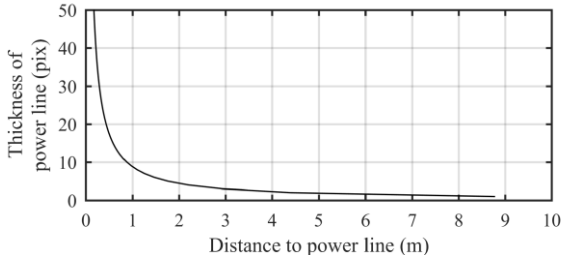

Figure 8. Thickness of a 35-mm power line in an image versus distance.

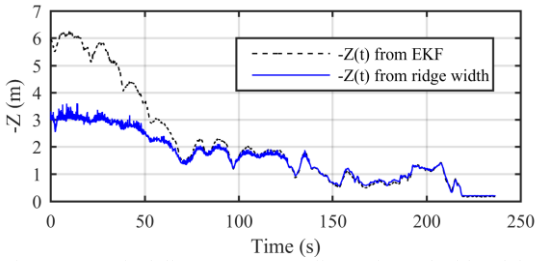

Figure 9. Vertical distance to power line estimated with solely $[w]_I$ versus with the EKF using $[\mathbf{D}]_L$ and $[\mathbf{L}]_I$.

Two sets of results are shown with two different ways of using the camera and LiDAR measurements in the EKF. The first set are from images taken on a cloudy day while the second are from ones taken on a sunny day. Wind speed was below 10 km/h. In both sets, controller gain was adjusted to obtain a damped response while providing a good tradeoff between settling time and noise sensitivity. The Pixhawk used its IMU and barometer to stabilize the UAV. Images were processed at a rate of 30 frames per seconds. Average processing time for one image is 20±6 ms.

1) Landing under ideal conditions

In cloudy weather, the LiDAR functioned consistently throughout the landing so only the LiDAR measurement $[\mathbf{D}]_L$ and power line projection in the image $[\mathbf{L}]_I$ were used in the EKF. The ridge width measurement $[w]_I$ was not used.

The pilot brings the UAV to a position about 6 m above and 1.5 m to the left of the power line. The controller then takes over and centers the UAV on the power line in about 5 seconds. During slightly less than 4 minutes, the pilot gradually lowers the UAV towards the power line and moves it forward and backward by about 2 m. Figures 9 to 12 show the path of the UAV. At a distance to the power line of less than 1.7 m, the root mean square error along the lateral ($\mathbf{Y}_P$) axis is 61 mm and the maximum error is 220 mm. The UAV stays aligned with the power line with a yaw angle varying between +2.3° and –7.6°. After the landing, ridge detector bias due to shadows lead to a yaw angle of 0.87°. The error remains conducive to safely landing the vehicle on the power line.

2) Landing under more challenging light conditions

The second set of results is from images taken on a sunny day. LiDAR measurements were not consistent above 2.5 m. Though the camera cannot accurately measure power line width above 1.7 m, it is still used for measuring the distance to the power line at higher altitudes. At higher altitudes, the ridge detector overestimates the ridge width and so underestimates the altitude of the UAV. Underestimating the altitude means that the lateral position of the UAV relative to the power line is also underestimated. The controller then takes more time than expected to converge above the power line. As the UAV descends towards the power line, the ridge width becomes more and more accurate. At 1.7 m, the ridge width is correctly measured and thus the altitude correctly determined.

The EKF uses LiDAR and camera measurements as follows. Above an altitude of 1.7 m, measurement vector $\mathbf{Z}$ consists of the ridge width $[w]_I$ and power line in image $[\mathbf{L}]_I$. Below an altitude of 1.3 m, $\mathbf{Z}$ consists of $[\mathbf{D}]_L$ and $[\mathbf{L}]_I$.

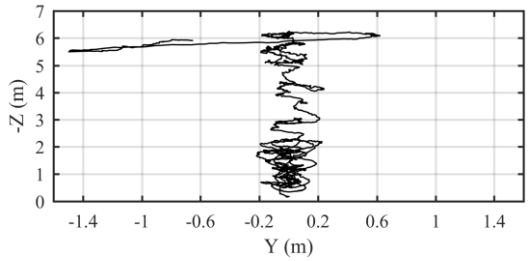

Figure 10. Estimated path of the UAV during hover and landing in the ($\mathbf{Y}_P$, $\mathbf{Z}_P$) plane in cloudy weather.

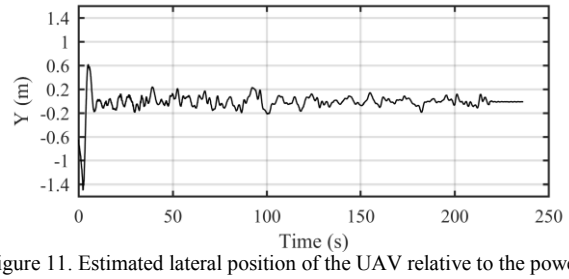

Figure 11. Estimated lateral position of the UAV relative to the power line during hover and landing in cloudy weather.

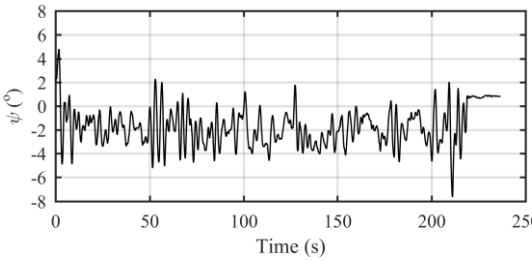

Figure 12. Estimated yaw of the UAV relative to the power line during hover and landing in cloudy weather.

The pilot needs to bring the UAV below 1.3 m to activate the LiDAR measurements and above 1.7 m to deactivate the LiDAR and reactivate the ridge width. Switching between LiDAR and ridge width is thus done with a hysteresis.

Figures 13 to 16 show the path of the UAV during landing. The controller was activated at about 10 m above the power line. At first, the estimated altitude saturates around 2.5 m because the camera and ridge detector are not sensitive enough to measure the ridge width. Below 2.5 m, the altitude begins to vary until 1.3 m, where the LiDAR starts and the ridge width stops being used. Because LiDAR and camera both measure the correct distance to the power line, the transition between the two sensors does not introduce any perturbation in the estimate of the pose of the camera. At 60 seconds, the UAV lands on the power line. Since the power line was lit uniformly during the experiment, the yaw angle is about 0° after landing.

VII. Conclusion

This paper presented a UAV, a vision system and a control strategy capable of bringing a new set of tools onto a power transmission line in order to perform non-destructive testing. Test results demonstrate landing on a non-energized line. Despite specific camera and LiDAR limitations, measurements from both can be combined in an extended Kalman filter that estimates the pose of the UAV relative to the power line.

The next step in the project will be to demonstrate landing on an energized line. Further work will also be directed toward characterizing and optimizing system performance under higher wind conditions. The vision system can be improved by making ridge width measurements more accurate at higher altitudes and less sensitive to differences in power line illumination. A higher frame rate should also be achievable. As the system is being tested on different sites, the robustness of the approach to more challenging backgrounds will be better studied and improved. Lastly, new payloads are currently under development to target additional high-value missions for the power industry.

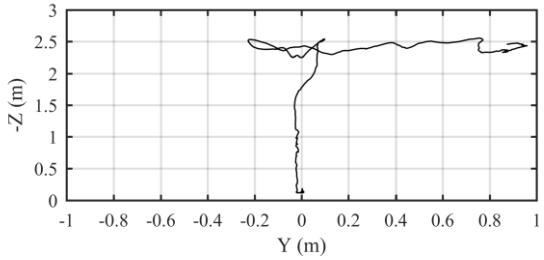

Figure 13. Estimated path of the UAV during landing in sunny weather.

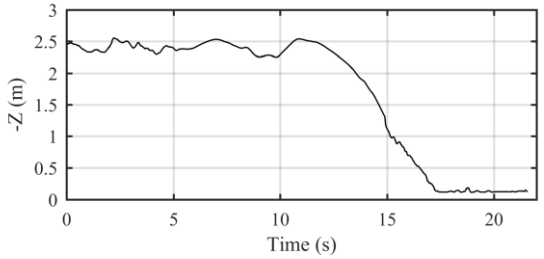

Figure 14. Estimated altitude of the UAV relative to the power line during landing in sunny weather.

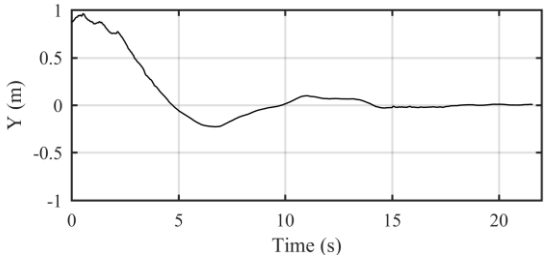

Figure 15. Estimated lateral position of the UAV relative to the power line during landing in sunny weather.

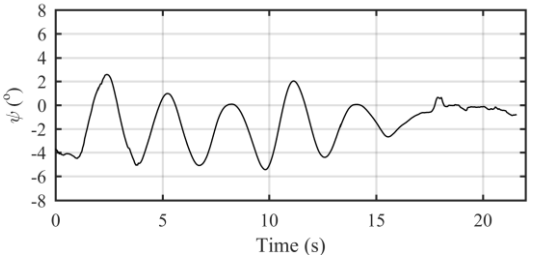

Figure 16. Estimated yaw of the UAV relative to the power line during landing in sunny weather.

REFERENCES

[1] R. A. Fernandes, "Monitoring system for power lines and right-of-way using remotely piloted drone," U.S. Patent 4 818 990A, April 4, 1989.

[2] H.W. Wopereis, J.J. Hoekstra, T.H. Post, G.A. Folkertsma, S. Stramigioli, and M. Fumagalli, "Application of substantial and sustained force to vertical surfaces using a quadrotor," in *Proc. IEEE Int. Conf. on Robotics and Automation (ICRA)*, 2017, pp. 2704–2709.

[3] D. R. McArthur, A. B. Chowdhury, and D. J. Cappelleri, "Design of the I-BoomCopter UAV for environmental interaction," in *Proc. IEEE Int. Conf. on Robotics and Automation (ICRA)*, 2017, pp. 5209–5214.

[4] N. Pouliot, G. Rousseau, A. Leblond, and S. Montambault, "Portable X-ray system for in situ detection of broken ACSR strands at suspension clamps: field results and equipping the LineScout robot," in *CIGRÉ 2016 Symposium,* B2-206, Paris, France.

[5] N. Pouliot and S. Montambault , "Field-oriented developments for LineScout technology and its deployment on large water crossing transmission lines," *J. of Field Robotics*, vol. 29, no. 1, pp. 25–46, 2012.

[6] E. Lavoie, G. Rousseau, N. Pouliot, and S. Montambault; "Hydro-Québec's LineCore technology – Probing below the surface," *Transmission & Distribution World*, in press.

[7] J. Moore and R. Tedrake, "Powerline perching with a fixed-wing UAV," in *Proc. AIAA Aerospace Conf.*, Seattle, Washington, 2009, pp.1–16.

[8] J. Thomas, G. Loianno, K. Daniilidis, and V. Kumar, "Visual servoing of quadrotors for perching by hanging from cylindrical objects," *IEEE robotics and automation letters*, vol. 1, no. 1, pp. 57–64, 2016.

[9] I. Sa and P. Corke, "Close-quarters quadrotor flying for a pole inspection with position based visual servoing and high-speed vision," in *Proc. IEEE Int. Conf. on Unmanned Aircraft Systems (ICUAS)*, 2014, pp. 623–631.

[10] I. Sa, S. Hrabar, and P. Corke, "Inspection of pole-like structures using a vision-controlled VTOL UAV and shared autonomy," in *Proc. Int. Conf. on Intelligent Robots and Systems*, pp. 4819–4826, 2014.

[11] I. Sa, S. Hrabar, and P. Corke, "Outdoor flight testing of a pole inspection UAV incorporating high-speed vision," *Field and Service Robotics*, vol. 105, pp. 107–121, 2015.

[12] Z. Li, Y. Liu, R. Walker, R. Hayward, and J. Zhang, "Towards automatic power line detection for a UAV surveillance system using pulse coupled neural filter and an improved Hough transform," *Machine Vision and Applications*, vol. 21, no. 5, pp. 677–686, 2010.

[13] Y. Liu, L. Mejias, and Z. Li, "Fast power line detection and localization using steerable filter for active UAV guidance," *Int. Archives of the Photogrammetry, Remote Sensing and Spatial Information Sciences*, Vol. XXXIX-B3, 2012.

[14] B. Song and X. Li, "Power line detection from optical images," *Neurocomputing*, vol. 129, pp. 350–361, April 2014.

[15] A. Ceron, I. F. Mondragon, and F. Prieto, "Power line detection using a circle based search with UAV images," in *Proc. IEEE Int. Conf. on Unmanned Aircraft Systems (ICUAS)*, 2014, pp. 632–639.

[16] C. Steger, "An unbiased detector of curvilinear structures," *IEEE Transactions on Pattern Analysis and Machine Intelligence*, vol. 20, no. 2, pp. 113–125, 1998.

[17] D. Langenegger, "Cable installation inspection vehicle and cable installation inspection method," European Patent EP2983259A1, Feb. 10, 2016.

[18] Skive Aviation AG. (2015). Skive power line robot. [Vimeo video]. Available: https://vimeo.com/138332266. Accessed July 12, 2017.

[19] MIR Innovation, Hydro-Quebec. Unmanned aerial vehicle (UAV) landing on a 315 kV test bench. [YouTube video] Available: https://youtu.be/RgmUvay3BwA. Accessed July 16, 2017.

[20] Pixhawk.org. (2017). Pixhawk Flight Controller Hardware Project [Online]. Available: https://pixhawk.org. Accessed July 27, 2017.

[21] R. Hartley and A. Zisserman, *Multiple View Geometry in Computer Vision*. Cambridge University Press, 2003.

[22] Y. Bar-Shalom and T. E. Fortman, *Tracking and Data Association*, Mathematics in Science and Engineering, vol. 179, Academic Press, 1988.

[23] Ardupilot.org. (2017). *ArduPilot Open Source Autopilot* [Online]. Available: http://ardupilot.org. Accessed July 27, 2017.

[24] Mavlink.org. (2017). MAVLink Micro Air Vehicle Communication Protocol [Online]. Available: http://mavlink.org. Accessed July 27, 2017.

[25] C. Teulière, L. Eck, and E. Marchand; "Chasing a moving target from a flying UAV", in *Proc. IEEE/RSJ Int. Conf. on Intelligent Robots and Systems*, 2011, pp. 4929–4934.